

Article

Comprehensive Computational Model for Coupled Fluid Flow, Mass Transfer, and Light Supply in Tubular Photobioreactors Equipped with Glass Sponges

Albert Mink^{1,2}, Kira Schediwy³, Clemens Posten³, Hermann Nirschl¹, Stephan Simonis^{2,4,*} 
and Mathias J. Krause^{1,2,4} 

¹ Institute for Mechanical Process Engineering and Mechanics, Karlsruhe Institute of Technology, 76131 Karlsruhe, Germany

² Lattice Boltzmann Research Group, Karlsruhe Institute of Technology, 76131 Karlsruhe, Germany

³ Institute of Process Engineering in Life Sciences, Karlsruhe Institute of Technology, 76131 Karlsruhe, Germany

⁴ Institute for Applied and Numerical Mathematics, Karlsruhe Institute of Technology, 76131 Karlsruhe, Germany

* Correspondence: stephan.simonis@kit.edu

Abstract: The design and optimization of photobioreactor(s) (PBR) benefit from the development of robust and quantitatively accurate computational fluid dynamics (CFD) models, which incorporate the complex interplay of fundamental phenomena. In the present work, we propose a comprehensive computational model for tubular photobioreactors equipped with glass sponges. The simulation model requires a minimum of at least three submodels for hydrodynamics, light supply, and biomass kinetics, respectively. First, by modeling the hydrodynamics, the light–dark cycles can be detected and the mixing characteristics of the flow (besides the mass transport) can be analyzed. Second, the radiative transport model is deployed to predict the local light intensities according to the wavelength of the light and scattering characteristics of the culture. The third submodel implements the biomass growth kinetic by coupling the local light intensities to hydrodynamic information of the CO₂ concentration, which allows to predict the algal growth. In combination, the novel mesoscopic simulation model is applied to a tubular PBR with transparent walls and an internal sponge structure. We showcase the coupled simulation results and validate specific submodel outcomes by comparing the experiments. The overall flow velocity, light distribution, and light intensities for individual algae trajectories are extracted and discussed. Conclusively, such insights into complex hydrodynamics and homogeneous illumination are very promising for CFD-based optimization of PBR.

Keywords: computational fluid dynamics; radiative transport; lattice Boltzmann method; photobioreactors; numerical simulation



Citation: Mink, A.; Schediwy, K.; Posten, C.; Nirschl, H.; Simonis, S.; Krause, M.J. Comprehensive Computational Model for Coupled Fluid Flow, Mass Transfer, and Light Supply in Tubular Photobioreactors Equipped with Glass Sponges. *Energies* **2022**, *15*, 7671. <https://doi.org/10.3390/en15207671>

Academic Editor: Jack Legrand

Received: 21 September 2022

Accepted: 15 October 2022

Published: 18 October 2022

Publisher's Note: MDPI stays neutral with regard to jurisdictional claims in published maps and institutional affiliations.



Copyright: © 2022 by the authors. Licensee MDPI, Basel, Switzerland. This article is an open access article distributed under the terms and conditions of the Creative Commons Attribution (CC BY) license (<https://creativecommons.org/licenses/by/4.0/>).

1. Introduction

Through the establishment of photobioreactor(s) (PBR) with optimized light characteristics, microalgae are renewable and cost-effective alternatives for industrial feedstock. Based on the following reasoning, the optimization of light characteristics is crucial. Along the light path, the algae become more limited in growth by the insufficient light supply due to the algal absorption and scattering behavior. In contrast, algae close to the reactor surface are subjected to light saturation or even photoinhibition. These effects increase the relative proportion of respiration and heat dissipation, respectively. The consequential loss of energy reduces biomass growth and is not favorable for industrial processes. Common approaches to overcome the (steep) light gradients are internal illuminations [1], the straightforward reduction of the light path using more reactor units, the enlargement of the reactor surface, or the installation of light-diluting structures in the reactor [2]. All

named approaches aim for the enhancement of the surface-to-volume ratio [3]. The increased ratio causes lower light intensities on the reactor surface and shorter light paths on average, which in turn yields a more homogeneous light supply in the algal culture.

From an engineering perspective, the demand for a high surface-to-volume ratio can be covered by closed PBR due to the hardly-limited light setups. When designing such PBR with the help of computer simulations, the increased complexity in the light pattern cannot be met by the popular Lambert–Beer-based simulation models. Instead, new powerful simulation tools are needed [4] that are able to consider absorption and scattering in the prediction of general light transport in volume and thus help to speed up the design of novel, more efficient, and low-cost PBR. In addition to the improved light pattern in the reactor, higher mixing rates cause the algae to experience more uniform conditions throughout the reactor geometry. The frequent transfer between light zones can be regarded as a homogenization of light conditions and subsequently of the intracellular metabolic reactions. Such optimized flows along the light gradient can be initiated by, e.g., wall turbulence promoters. In computational fluid dynamics (CFD) simulations, turbulence promoters implemented as profiles at the inner tube wall establish better mixing behaviors at lower flow velocities, yielding a significantly reduced energy demand [5]. Further, adopting the principle of static mixers, the cultivation efficiency in flat-plate PBR has increased by optimizing the flow pattern using CFD simulations [6]. Lastly, novel reactor designs, such as the Taylor vortex PBR, also show that complex flow patterns lead to promising mixing behaviors [7]. The named simulations share the usage of algae trajectories to evaluate the mixing behaviors as the main characteristics.

Simulation tools for the light supply and the algae trajectories in PBR are advanced and already validate many algorithms, including the discrete ordinate method (DOM) [8], the Monte Carlo (MC) algorithm [9,10], and finite volume method (FVM) [11] for light supply, and various Euler–Lagrange models for the trajectories [5,12,13]. Nevertheless, the combination of models for coupling the light supply with the algae trajectories (eventually taking additional mass transfer into account) remains a numerical challenge. This often leads to simplified and inaccurate light predictions, considering algebraic light models based on Lambert–Beer and others [6,14,15].

The inaccuracy of complete PBR simulations limits the progress in the reactor design and process development. However, this progress is highly desirable from various perspectives and is essential for covering the increasing demand of bio-based resources. Consistent numerical frameworks that model (at least) the light supply, hydrodynamics, and biomass growth kinetics, may play important roles in the development of accurate and reliable predictions, see Figure 1. Further, the numerical approach renounces complicated coupling and time-consuming data interpolation. Numerical tools might also speed up the prototyping of novel and complex reactor designs and analyze the interplay of the flow field, light supply, and mass transfer to determine the reactor performances.

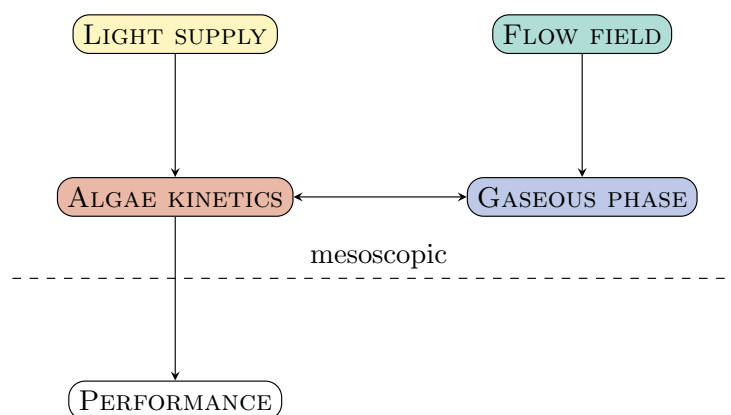


Figure 1. Interconnect model of the flow field, light supply, and mass transfer.

In previous works by Mink et al. [16–18], the light transport simulation based on the lattice Boltzmann method (LBM) was extended, validated, and applied to efficiently predict light distribution in PBR. As an alternative approximation technique in CFD, an LBM simulation has a particular strength in multiphysics applications [19–34], and is a suitable framework for the development of a computational model for algae trajectories (Lagrange–Lagrange) and mass transfer (Euler–Lagrange). In addition, LBM brings forth almost perfect parallelizability, which allows highly scalable simulations on high-performance computing machinery. Under the premise of the prolific features of LBM, the above-motivated full-scale PBR simulations with fairly accurate models become feasible. As a completion of the previous developments [16–18], this work proposes a joint, comprehensive, three-dimensional simulation model for light supply, flow pattern, and mass transfer using a numerical framework based on LBM. The model is implemented in the open-source C++ framework OpenLB [35,36] and applied to digitally twin a tubular PBR equipped with transparent sponges. We evaluated the overall computational results, as well as specific quantities of individual model components, and compared the latter them to experimental measurements of light intensities within the PBR. Altogether, we find good agreement with the reference experiments.

In summary, the objectives of this paper are as follows.

- We propose a coupled, comprehensive, spatially three-dimensional simulation model for light supply, flow pattern, and mass transfer based on LBM.
- We implemented the model in the open-source parallel C++ framework OpenLB.
- We showcase the coupled simulation results for PBR with internal glass sponges.
- We assessed the individual model results quantitatively via comparison to experiments.
- We discuss the simulation results with respect to other simulation approaches [4].

The rest of the paper is organized as follows. Section 2 summarizes the methodology for the model components. The computational setup and results are presented in Sections 3 and 4. Finally, a conclusion is drawn in Section 5.

2. Materials & Methods

2.1. Description of the Glass Sponge PBR

One way to improve the light pattern in microalgal cultures is the installation of transparent polyurethane sponges in a PBR. Jacobi et al. [2] applied these open-pored sponges to a flat panel PBR, where the manufacturing was based on the polymer replica technique. Two major effects allow the sponges to improve the reactor performance compared to liquid cultures without built-in structures:

- (i) The so-called light dilution is achieved by increasing the illumination area by the surface area of the sponges in addition to the surface area of the PBR itself. The sponges conduct light to deeper positions (Figure 2) in the PBR and also decrease the light path in the microalgal culture.
- (ii) Algae grow within the pores of the sponges and become illuminated from all directions due to the multiple and complex reflections in the glass sponges. The illumination from all directions toward the center of each pore focuses the light, as shown in Figure 3. This focus effect counteracts the attenuation of light due to the scattering and absorption of algae along the light path.

Both effects cause more homogeneous or less extreme light intensities compared to liquid cultures in an analogous geometry without sponges since the attenuation of light shows less decay within the shorter path.

In this work, we applied the glass sponges to a tubular PBR. The dimensions of the simulated geometry were 0.05 m in diameter and 0.05 m in length, while the initial flow rate was 0.01 m/s. Due to computational limitations, the characteristics of the sponges were scaled up by a factor of 10 compared to the above-mentioned study with 8 pores per

inch, the porosity of 0.9, and the specific surface area of $568 \text{ m}^2/\text{m}^3$. The absorption of light in the glass remained below $0.1/\text{m}$.

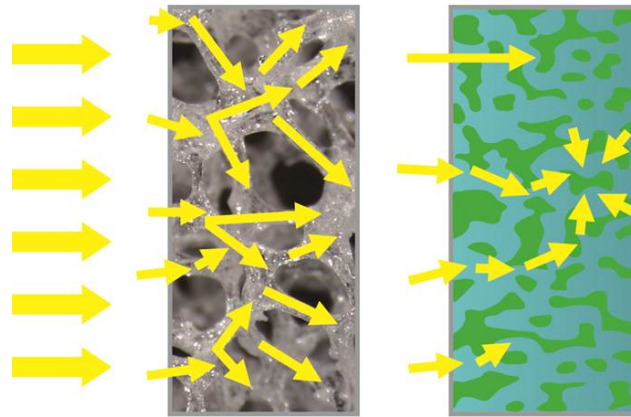


Figure 2. Photograph (left) of a transparent sponge with light transmission and the scheme (right) of the resulting focus effect due to the illumination of the volume in the pores from all directions. Reprinted/adapted with permission from Ref. [2]. Copyright 2012 Jacobi A, et al.

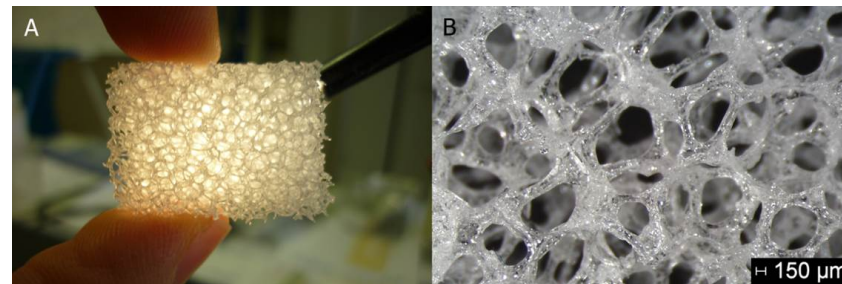


Figure 3. Photograph (A) and high-resolution image (B) of a transparent sponge show deep and homogeneous light transmissions in the glass structure. Reprinted/adapted with permission from Ref. [2]. Copyright 2012 Jacobi A, et al.

2.2. Mesoscopic Modeling and the Lattice Boltzmann Method

A crucial difference between the LBM compared to traditional numerical schemes, such as FVM, is the modeling and simulation scale. Unlike traditional schemes that solve discretized macroscopic equations, the LBM arises from kinetic theory and the Boltzmann equation, where collision rules are defined on a mesoscopic level [37,38]. The mesoscopic scale is a stochastic abstraction of the particle-based microscopic level. The law of large numbers ensures asymptotically that the mesoscopic collision rule solves macroscopic (target) equations. LBM is well-known for intuitive modeling, intrinsically parallelizable algorithms, the ability to address complex boundary conditions, and multiphysics models [39,40].

2.3. Light Distribution Model

The light transport in a spatially homogeneous medium is governed by the radiative transport equation (RTE)

$$\frac{1}{c} \partial_t L + \mathbf{s} \cdot \nabla L = -(\mu_a + \mu_s)L + \mu_s \int_{\Omega} \tilde{p}(\mathbf{s}', \mathbf{s}) L(t, \mathbf{x}, \mathbf{s}') d\Omega' \quad (1)$$

which models the loss or radiance L due to absorption μ_a and the redistribution of radiance by scattering μ_s . Equation (1) describes the change of mesoscopic intensity of light L in time along a path element \mathbf{s} . To model algae suspensions, we used case-specific absorption

and scattering coefficients and a scattering integral with the phase function \bar{p} [41,42]. Inside a small control volume at position x , the local light intensity Φ is obtained by

$$\Phi(t, x) = \int L(t, x, s) d\Omega. \quad (2)$$

Note that the RTE (1) is formulated with respect to a certain wavelength λ , which is dropped for the sake of simplicity. In previous works, Mink et al. [16,17] established the radiative transport LBM (RTLBM) as a numerical tool to solve the general RTE. Here, we employ the RTLBM to approximate (1) and, thus, to recover the local light intensity (2).

Spectral light regimes are typically approximated by the Box model, where the RTE is solved for several wavelengths and the computed intensities are averaged [43,44]. This extension might be of interest when improving the light utilization efficiency since not all absorbed light in the visible spectrum contributes equally to the conversion to biomass. Inhomogeneous suspensions are modeled by spatially varying optical parameters μ_a and μ_s . The parameter values rise with locally increased biomass concentrations and vice versa. In addition, light sources of arbitrary shapes and numbers can be added by introducing corresponding source terms in the Box model.

The optical characterization of algae suspension with respect to scattering and absorption properties is a non-trivial experimental task. Measurements depend on the wavelength and growth conditions, e.g., see Table 1. Moreover, the scattering must be analyzed within thin suspensions to avoid multiple scattering events that would blur the analysis of one single scattering event [45–47]. Bubbles in the suspension are not considered here, since the influence on the light supply is negligible as shown in previous experimental and numerical works [47,48].

Table 1. Experimentally obtained absorption and scattering cross-sections of *C. reinhardtii* under optimal growth conditions. Data and notation are summarized from [49].

λ in nm	$\hat{\mu}_a$ in m ² /kg	$\hat{\mu}_s$ in m ² /kg
470	400	800
600	140	1700
680	380	1300

Fresnel's and Snell's law for modeling the reflection and transmission on surfaces induces the following boundary condition. The radiance that hits a boundary surface with an angle θ is reflected and attenuates according to Fresnel's equation. If the incident angle is greater than the critical angle θ_c , then the intensity is reflected (with reflectance $R_F = 1$) and there is no transmission, otherwise, the incident radiation is multiplied by Fresnel's equation

$$R_F(\theta) = \frac{1}{2} \left(\frac{n_{rel} \cos \theta_r - \cos \theta}{n_{rel} \cos \theta_r + \cos \theta} \right)^2 + \frac{1}{2} \left(\frac{n_{rel} \cos \theta - \cos \theta_r}{n_{rel} \cos \theta + \cos \theta_r} \right)^2, \quad \text{for } 0 \leq \theta \leq \theta_c, \quad (3)$$

which results in an attenuation factor due to reflection and transmission. The parameter n_{rel} accounts for the reflection properties of the surface and θ_r is the refraction angle according to Snell's law [18].

In the framework of RTLBM, this boundary condition translates into a partial bounce-back scheme [18]. Based on the reflection properties of the reactor surface manifested in n_{rel} , a physical description of a partial bounce-back coefficient is determined, which models the partial reflection due to Fresnel's Equation (3).

2.4. Fluid Flow Regime and Lagrangian Particles

The fluid flow is governed by the incompressible Navier–Stokes equations (NSE)

$$\begin{cases} \partial_t \mathbf{u} + (\mathbf{u} \cdot \nabla) \mathbf{u} = -\frac{\nabla p}{\rho} + \nu \nabla^2 \mathbf{u}, \\ \nabla \cdot \mathbf{u} = 0, \end{cases} \quad (4)$$

with fluid velocity \mathbf{u} , density ρ , pressure p , and kinematic viscosity ν . Equation (4) is approximated with LBM [32] and implemented in the parallel, open-source C++ framework, OpenLB [35,36]. To account for the turbulence, a large-eddy simulation model replaces the viscosity ν in (4) with a local effective viscosity that additionally models the non-resolved scales [19] through a Smagorinsky–Lilly approach. Due to a mesh-sized filter width, the turbulence in the flow regime is either modeled or resolved, depending on the scale yielding a consistent numerical scheme. Additionally, the LBM's intrinsic parallelizability ensures a completely local and, thus, efficient computation of the additional LES parameters.

Individual algae trajectories are computed according to a Euler–Lagrange approach. Single algae are modeled as Lagrangian point particles of mass m_P and tracked according to Newton's second law of motion

$$m_P \partial_t \mathbf{u}_P = \mathbf{F}_P \quad (5)$$

for a general force \mathbf{F}_P . Due to the small characteristic size of microalgae (2 μm to 10 μm), the Stokes drag force

$$\mathbf{F}_P = \frac{\pi r_P^2}{2} \rho_P C_D (\mathbf{u}_F - \mathbf{u}_P) \quad (6)$$

offers a suitable description, where C_D is the drag coefficient, r_P denotes the particle radius and ρ_P is the particle density. LBM-specific implementation details are given in [50].

The present Euler–Lagrange approach using (5) and (6) assumes that algae do not affect the fluid flow, which is valid for commonly used biomass concentrations in tubular PBR. In summary, despite its simplicity, the model allows us to study the time evolution of a representative population of algae in the fluid flow and to draw conclusions about trapped algae in vortices, the quality of mixing, and the induced shear stress [13], respectively.

2.5. Mass Transport

The Euler–Euler approach models the mass transport of a species or concentration c in a flow field \mathbf{u}_F via the advection–diffusion equation

$$\partial_t c = D \nabla^2 c - \nabla \cdot \mathbf{u}_F c + R, \quad (7)$$

where D is the diffusivity and the advection velocity \mathbf{u}_F couples to the fluid flow modeled by the NSE. Here, c is the CO_2 concentration. The sink term R in (7) accounts for the consumption due to the photosynthetic conversion, which is specified below as a linear function of the photo-conversion rate. The term R relates the local light intensities to the available gas concentration.

Within the present model, Equation (7) is approximated with LBM. The top-down construction of LBM for partial differential equations akin to (7) and rigorous convergence proofs are established in [24,30]. Note that the LBM framework used here for a coupled equation system, such as (4) and (7), has been presented and validated previously for particle flow by Trunk et al. [20].

2.6. Algae Growth Model and Coupling

The PBR simulation model connects the local light intensities to the gas transport, by means of CO_2 consumption $\partial_t c$ according to the (local) rate of photosynthesis. Here,

a Monod model that assumes a light-limited biomass growth was implemented. Based on that, the rate of photosynthesis is computed by

$$P = P_{max} \frac{L}{L_K + L} \quad (8)$$

for a maximal photosynthesis rate P_{max} and a constant L_K . Further, we expect a linear connection of specific biomass growth and photosynthesis rate (8). More complex biomass growth models, accounting for multiple substrate factors and temperatures, are discussed for example in [51–53]. However, the trade-off between many empirical parameters and comprehensive modeling has to be managed carefully.

On the mesoscopic scale, the local light information is available and the photosynthesis rate is computed easily. This information is coupled to the CO₂ transport by the sink term R , as mentioned earlier, and represents gas consumption. All computational operations are strictly local and retain the perfect parallelizability of LBM.

3. Results

3.1. Geometry and Computational Parameters

The simulated tubular PBR has a diameter of 0.05 m and length of 1 m, where the sponge structure is placed at 0.5 m from the inlet. When simulating tubular geometries, the hydrodynamics develop after the inlet and are required to settle to avoid numerical errors. To this end, the tube is extended artificially to allow the development of the flow pattern.

The spatial discretization of both fine and coarse structures through a regular grid comes with a trade-off of maximal possible grid nodes or lattice cells and the staircase approximation of the fine structure. Due to memory and computation time limitations, the pore sizes of 0.002 m to 0.004 m from the original experiments [2] cannot be resolved. However, the present work considers a pore size of 0.02 m, which is resolved by a grid size of 5×10^{-4} m, yielding an overall number of 1.5×10^7 lattice cells. Compared to the original pore sizes of approximately 0.003 m in [2] the present pore size increased by about a factor of 10.

Concerning the hydrodynamics, the flow enters as a Poiseuille profile with a mean velocity of 0.01 m/s and a viscosity of 1×10^{-5} kg/(m s). The pressure boundary at the end of the channel ensures a physically sound outflow boundary condition, whereas all other walls are modeled as no-slip walls by the LBM bounce-back scheme. Figure 4 shows the geometry of the PBR with the sponge structure and the simulated flow field, light supply, and mass transfer.

3.2. Simulation Sequence

First, the RTLBM light simulation is carried out to approximate (1). The photo-translucent sponge (with the tubing) acts as a radiative source of constant light intensity. Afterward, the fluid field is simulated by approximating the coupled system (4) and (7) for a Poiseuille inflow profile and no-slip walls with vanishing fluid velocity. Since the entire geometry is provided as an STL file, the interpolated bounce-back model of Bouzidi et al. [54] is deployed. The interpolated boundary method offers robustness in terms of stability for the staircase approximation of the sponge structure. Finally, after the full flow pattern is developed, the algae cells are added and tracked according to the Euler–Lagrange approach described in Section 2.4.

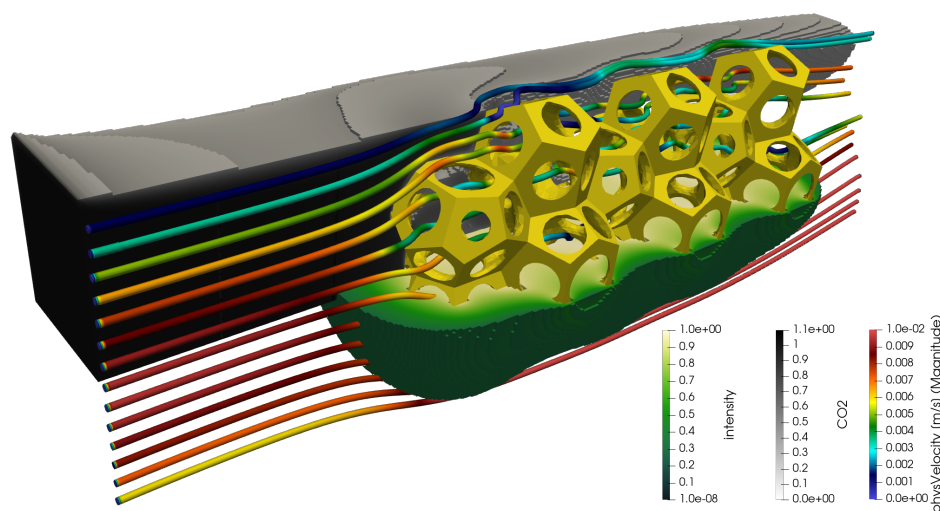


Figure 4. Coupled simulation result of flow hydrodynamics, gas transport, and light distribution in a complex PBR with internal sponge structure.

3.3. Validation of Light Simulation

For validation purposes, we measured the light intensities in a diluted microalgal suspension. The low biomass concentration minimizes the number of scattering and absorption events and maximizes the spatial resolution compared to the sensor's size. The planar mini quantum sensor (Walz, LS-C, diffuser diameter 0.003 m) quantifies the photosynthetic active radiation (PAR), which is emitted by a warm white LED (Nichia, NS6L183BT). The LED is located in a glass tube to allow light propagation into the suspension. This radial setup causes light gradients along the radius even without algae. The algal absorption and scattering induce additional attenuation. To clearly differentiate these effects, the glass tube is partially covered, which prevents undesired reflection on the glass surface. For all measurements, the planar sensor is oriented towards the center of the long axis of the glass tube. The measuring configuration allows shifts in a longitudinal direction, variations of the radius up to 0.05 m, and an angular displacement of 10° around the entire glass tube, as indicated in Figure 5. The measurements and the corresponding three-dimensional simulations are performed for a biomass concentration of $9 \times 10^{-5} \text{ g/m}^3$.

The comparison of the data sets along the radius at 0° is exemplarily shown in Figure 6. The agreement of the simulation results with the measured data is especially convincing above 1% of the incident light intensity being $<3 \mu\text{mol}/(\text{m}^2 \text{ s})$. The light intensities in this order of magnitude are too low to sufficiently contribute to the algal growth or maintain the requirements of the cells. Consequently, the low intensities should not appear in a PBR and do not substantially impact consecutive growth models. The light model is validated and suitable for more complex geometries using the same optical principles and characteristics of the cells.

3.4. Light Simulation of Complex Geometry

Light simulation results of the tubular PBR with and without embedded sponges are depicted as a contour plot in Figure 7. To evaluate the general effect of the sponges in the tubular PBR, two ideal scenarios are compared. In an ideal theoretical setup, a certain light intensity radiates from the PBR wall and the sponges completely into the culture. The incident light intensity is considered independent of the intensity inside the sponge structure to achieve maximum homogenized conditions. Hence, the two possible scenarios are as follows.

- (i) The sponges and the tubular surface emit light at equal intensities.
- (ii) The same amount of photons per time as in (i) is emitted by the PBR surface only.

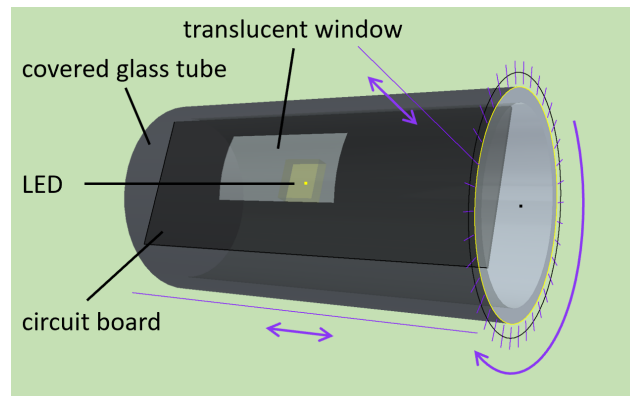


Figure 5. Experimental measurement configuration of the glass tube.

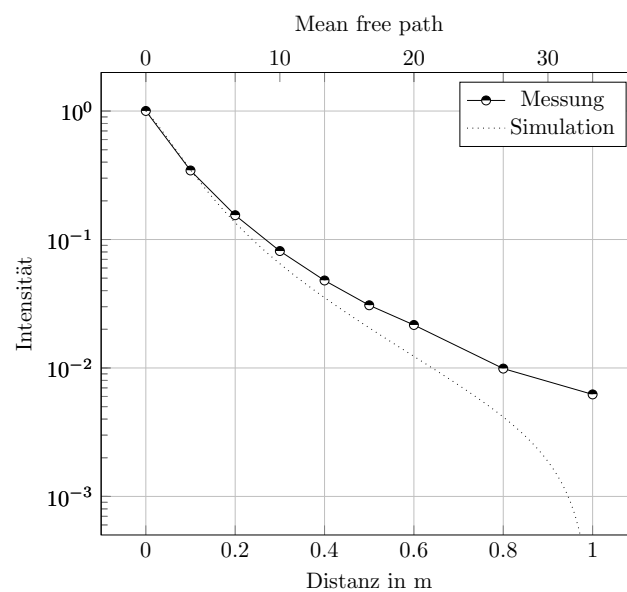


Figure 6. Comparison of simulated light intensity with experimental measurements.

Figure 7 (ii) compares where the light supply in the classic tube reactor is illuminated by its walls only (sections at the left and right ends of the tube) as well as (i) comprises the novel reactor with the internal sponge structure that dilutes the illumination into the suspension (the midsection of the tube). Without the sponges, the steep radial gradient shadows most of the suspension resulting in a heterogeneous light distribution with dark zones in the center of the tube. Close to the walls, the reactor volume is partly subjected to photo-saturation, which induces light limitation in deeper zones. Increasing the light intensity might reduce these dark zones. However, the higher incident light intensity might expose the suspension close to the light source to photo-inhibition, possibly yielding inefficient light use or even damage to the algal cells. Hence, the approach of increasing the light intensities translates the deficit to other reactor regions and barely solves the issue of heterogeneous light supply. In contrast to the latter, spreading the light sources over a larger surface and into deeper zones of the reactor via using the sponges homogenizes the light supply clearly, according to the simulations.

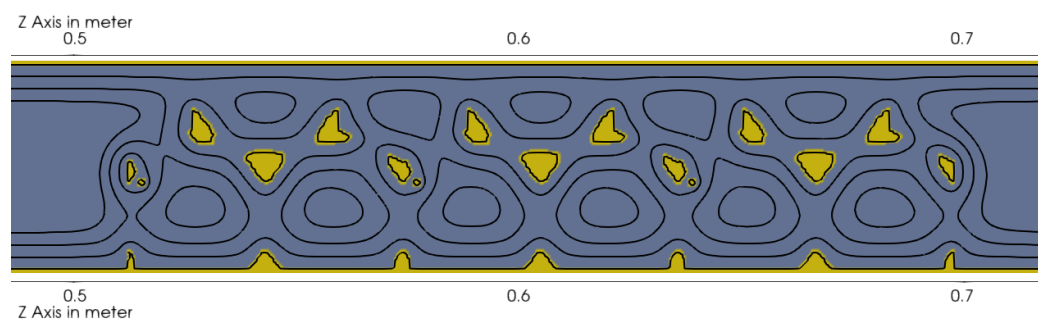


Figure 7. Contour lines on the light distribution. Yellow parts are light sources and the algae suspension is colored blue.

The implementation of a sponge structure inside the PBR is a promising strategy to homogenize the light distribution. The increase of the illuminating surface goes along with a reduction of the incident light intensity inversely proportional to the increase of the illumination surface. This so-called light dilution reduces both dark zones and zones of light saturation or even photoinhibition. A more homogeneous light supply enables higher biomass productivity. This effect is even more substantial in a real setup, since light gradients become steeper when illumination from the sun occurs from one side of the PBR only.

3.5. Fluid Flow Regime and Gaseous Transport

The sponge structure attains a complex flow pattern through the channel that enhances the radial mixing. While the fluid passes the sponge, the local constrictions lead to high velocities and a complex flow pattern develops for inlet velocities as slow as 0.01 m/s, see Figure 8.

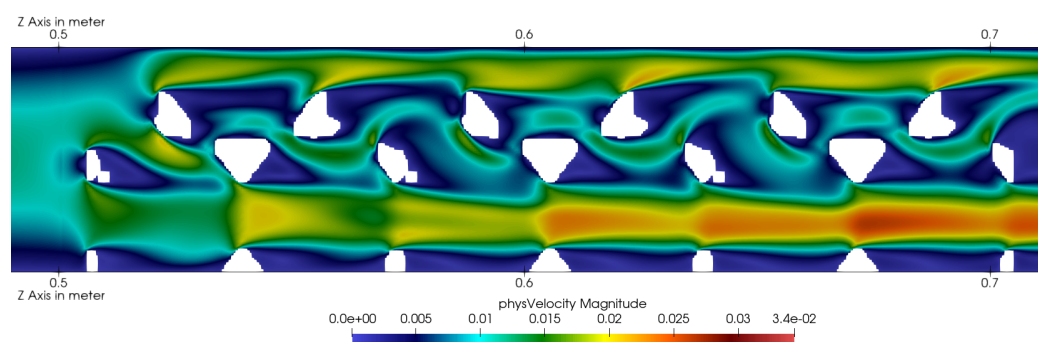


Figure 8. Local velocities for an inflow of 0.01 m/s. White regions are the sponge structure.

When the flow field is fully developed, the Lagrangian tracer particles are seeded randomly at the inlet and are tracked through the PBR. Figure 9 depicts the radial position of such algae cells in the reactor cross-section. The color gradient indicates the time evolution in the flow field from the beginning (dark) to the end (light). Along the trajectory, the algae are subjected to radial movements that indicate a non-laminar flow pattern and approve the mixing characteristics of the particular reactor design with built-in sponges. The information on the spatial positions is further analyzed by the locally subjected light intensities, which are depicted for the same tracer particles in Figure 10. Analyzing the algae light history along the z-direction, the sponge structure increases the general light supply clearly. Before and after the sponge structure, the subjected light decreases and remains at a constant level. The latter shows the laminar character of the flow field and how algae cells are not mixed and accordingly subjected to entirely different light regimes.

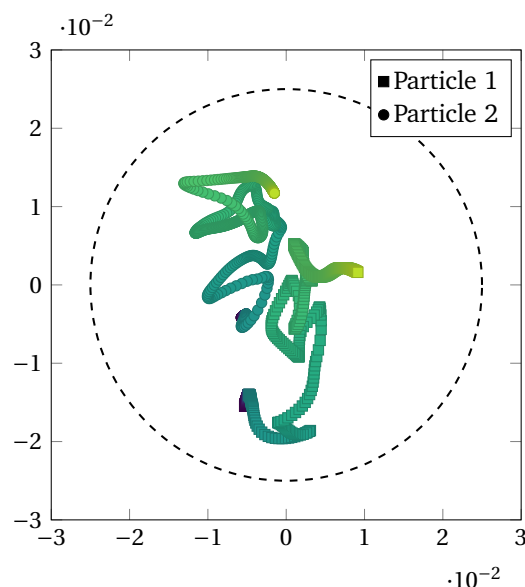


Figure 9. The cross-section of the tubular reactor shows the time evolution of two algae trajectories in the xy -plane. The trajectory starts are indicated by dark blue and the ends by light green, respectively.

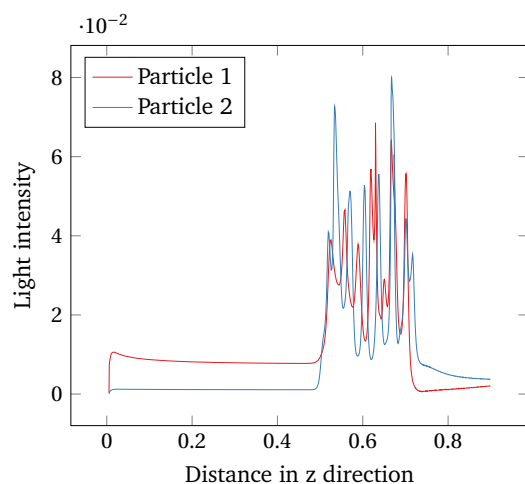


Figure 10. Experienced light intensity plotted over the traveled z -distance. The increase of subjected light intensity at the z -position 0.5 m is due to the sponge structure. Before and after the sponge structure, the subjected light is constant.

3.6. Biomass Growth

Figure 10 accounts for the light that the algae is exposed to in the flow field. Conducting a survey that considers the light history over time might indicate the presence of light–dark cycles and the precise frequency. However, the present data only indicate the tendency to light–dark cycles given the alternating light exposure history in Figure 10. The modeling of the trajectory (and its coupling to the light model) allows studying the light history of individual algae cells. The simulation data suggest that without the sponge structure, tubular reactors of a diameter of 0.05 m have poor radial mixing properties for fluid velocities of 0.01 m/s and lower. Further, in contrast to an empty tubular geometry, including the sponge structure increases both the mixing and the light exposure. Conclusively, the novel geometry used here will definitely lead to increased algal growth and, thus, optimize the biomass growth of the overall PBR.

4. Discussion

Concerning the effective biomass growth, we defer further examination of the light optimization by adding the sponge structure to future studies. However, additional factors

for the simulation outcome are likely. Varying the tube length of the PBR without the sponge structure, for example, should yield different results and might have a positive impact on the mixing if combined with higher fluid velocities. For example, Gupta [55] studied ellipsoidal particle paths for fully resolved pipe flows in tubular PBR at Reynolds numbers of about 3400 and obtained enhanced mixing and light intensities. Nevertheless, algae can be damaged at too-high Reynolds numbers, which in turn reduces the overall productivity of PBR [55]. From this point of view, it is again very promising to include sponge structures instead, which uphold high mixing and light intensities but allow lower flow velocities and shorter reactor geometries.

As existing models of complete PBR are highly differing in the assembly of the multi-physics simulation modules [4], a direct comparison of results is hardly possible. However, the present model recovers isolated key results from reference experiments. In particular, we compared the simulated light intensities in the model with experimental measurements of an actual tubular PBR setup, which led to good agreement above 1% of the incident light intensity. Nonetheless, the proposed model could be improved by including more physics, such as interphase mass transfer through a bubbly flow.

At last, the novelty of this study also induces its limitations. For the first time, we propose a complete framework for the three-dimensional kinetic simulation of photobioreactors based on LBM. We describe the model and provide qualitative and quantitative evaluations of the results. An actual practical implementation of the digital PBR twin to optimize, for example, a full-scale PBR geometry was not considered here. More elaborate research is required to validate the model for the application in complete PBR arrangements. Future studies should include the extensive practical usage of the here proposed model and its verification for geometry optimization purposes.

5. Conclusions

In the present work, we propose a comprehensive three-dimensional model for the numerical simulation of coupled light supply, flow pattern, and mass transfer. The model makes use of LBM and requires at least three submodels for hydrodynamics, light supply, and biomass kinetics, respectively. Subsequently to its methodological development, the novel mesoscopic simulation model is successfully applied to a tubular PBR equipped with an internal sponge structure. In particular, by modeling the hydrodynamics, the light-dark cycles are detected and the mixing characteristics of the flow (besides the mass transport) are analyzed. The radiative transport model is deployed to predict the local light intensities according to the wavelength of the light and scattering characteristics of the culture. The third submodel implements the biomass growth kinetic, by coupling the local light intensities to the hydrodynamic information of the CO₂ concentration, to predict the algal growth. We found good agreement in the experimental measurements and documented various simulation results for the individual submodels and the coupled PBR processes.

Future studies and model improvements are discussed above and suggested in [56]. CFD-based methods are very promising for the optimization of the complex hydrodynamics and homogeneous illumination in the design processes of PBR. Conclusively, the design, as well as the optimization of such reactors, benefit directly from the robust (and quantitatively accurate) computational model presented here, which incorporates the complex interplay of the governing transport dynamics in PBR.

Author Contributions: Conceptualization, A.M.; methodology, A.M., K.S. and S.S.; software, A.M. and M.J.K.; validation, A.M. and K.S.; formal analysis, A.M.; investigation, A.M. and S.S.; resources, C.P. and M.J.K.; data curation, A.M.; writing—original draft preparation, A.M. and S.S.; writing—review and editing, S.S.; visualization, A.M., K.S. and S.S.; supervision, M.J.K., C.P. and H.N.; project administration, A.M. and M.J.K.; funding acquisition, M.J.K. All authors have read and agreed to the published version of the manuscript.

Funding: This work was supported by the Deutsche Forschungsgemeinschaft (DFG) grant no. 322739165.

Data Availability Statement: All LBM computations in this work are conducted with the open-source parallel C++ framework OpenLB [36] (see [57] for the latest version).

Acknowledgments: This work was performed using the computational resources ForHLR I and ForHLR II, funded by the Ministry of Science, Research, and the Arts Baden-Württemberg and DFG (“Deutsche Forschungsgemeinschaft”). We acknowledge support from the KIT-Publication Fund of the Karlsruhe Institute of Technology.

Conflicts of Interest: The authors declare no conflict of interest.

References

1. Cornet, J.F. Calculation of optimal design and ideal productivities of volumetrically lightened photobioreactors using the constructal approach. *Chem. Eng. Sci.* **2010**, *65*, 985–998. [CrossRef]
2. Jacobi, A.; Bucharsky, E.C.; Schell, K.G.; Habisreuther, P.; Oberacker, R.; Hoffmann, M.J.; Zarzalis, N.; Posten, C. The Application of Transparent Glass Sponge for Improvement of Light Distribution in Photobioreactors. *J. Bioprocess. Biotech.* **2012**, *2*. [CrossRef]
3. Nwoba, E.G.; Parlevliet, D.A.; Laird, D.W.; Alameh, K.; Moheimani, N.R. Light management technologies for increasing algal photobioreactor efficiency. *Algal Res.* **2019**, *39*, 101433. [CrossRef]
4. Luzzi, G.; McHardy, C. Modeling and Simulation of Photobioreactors with Computational Fluid Dynamics—A Comprehensive Review. *Energies* **2022**, *15*, 3966. [CrossRef]
5. Gómez-Pérez, C.; Espinosa, J.; Ruiz, L.M.; van Boxtel, A. CFD simulation for reduced energy costs in tubular photobioreactors using wall turbulence promoters. *Algal Res.* **2015**, *12*, 1–9. [CrossRef]
6. Huang, J.; Feng, F.; Wan, M.; Ying, J.; Li, Y.; Qu, X.; Pan, R.; Shen, G.; Li, W. Improving performance of flat-plate photobioreactors by installation of novel internal mixers optimized with computational fluid dynamics. *Bioresour. Technol.* **2015**, *182*, 151–159. [CrossRef] [PubMed]
7. Gao, X.; Kong, B.; Vigil, R.D. CFD investigation of bubble effects on Taylor–Couette flow patterns in the weakly turbulent vortex regime. *Chem. Eng. J.* **2015**, *270*, 508–518. [CrossRef]
8. Kong, B.; Vigil, R.D. Simulation of photosynthetically active radiation distribution in algal photobioreactors using a multidimensional spectral radiation model. *Bioresour. Technol.* **2014**, *158*, 141–148. [CrossRef]
9. Csögör, Z.; Herrenbauer, M.; Schmidt, K.; Posten, C. Light distribution in a novel photobioreactor—Modelling for optimization. *J. Appl. Phycol.* **2001**, *13*, 325–333. [CrossRef]
10. Dauchet, J.; Blanco, S.; Cornet, J.F.; Hafi, M.E.; Eymet, V.; Fournier, R. The practice of recent radiative transfer Monte Carlo advances and its contribution to the field of microorganisms cultivation in photobioreactors. *J. Quant. Spectrosc. Radiat. Transf.* **2013**, *128*, 52–59. [CrossRef]
11. Huang, Q.; Liu, T.; Yang, J.; Yao, L.; Gao, L. Evaluation of radiative transfer using the finite volume method in cylindrical photoreactors. *Chem. Eng. Sci.* **2011**, *66*, 3930–3940. [CrossRef]
12. Perner-Nochta, I.; Posten, C. Simulations of light intensity variation in photobioreactors. *J. Biotechnol.* **2007**, *131*, 276–285. [CrossRef] [PubMed]
13. Lapin, A.; Müller, D.; Reuss, M. Dynamic Behavior of Microbial Populations in Stirred Bioreactors Simulated with Euler–Lagrange Methods: Traveling along the Lifelines of Single Cells. *Ind. Eng. Chem. Res.* **2004**, *43*, 4647–4656. [CrossRef]
14. Gao, X.; Kong, B.; Vigil, R.D. Comprehensive computational model for combining fluid hydrodynamics, light transport and biomass growth in a Taylor vortex algal photobioreactor: Lagrangian approach. *Bioresour. Technol.* **2017**, *224*, 523–530. [CrossRef] [PubMed]
15. Cornet, J.F.; Dussap, C.G. A simple and reliable formula for assessment of maximum volumetric productivities in photobioreactors. *Biotechnol. Prog.* **2009**, *25*, 424–435. [CrossRef]
16. Mink, A.; Thäter, G.; Nirschl, H.; Krause, M.J. A 3D Lattice Boltzmann method for light simulation in participating media. *J. Comput. Sci.* **2016**, *17*, 431–437. [CrossRef]
17. Mink, A.; McHardy, C.; Bressel, L.; Rauh, C.; Krause, M.J. Radiative transfer lattice Boltzmann methods: 3D models and their performance in different regimes of radiative transfer. *J. Quant. Spectrosc. Radiat. Transf.* **2020**, *243*, 106810. [CrossRef]
18. Mink, A.; Schediwy, K.; Haussmann, M.; Posten, C.; Nirschl, H.; Krause, M.J. Fresnel reflection boundary for radiative transport lattice Boltzmann methods in highly scattering volume. *arXiv* **2021**, arXiv:2107.09411.
19. Nathen, P.; Gaudlitz, D.; Krause, M.; Kratzke, J. An extension of the Lattice Boltzmann Method for simulating turbulent flows around rotating geometries of arbitrary shape. In Proceedings of the 21st AIAA Computational Fluid Dynamics Conference, San Diego, CA, USA, 24–27 June 2013.
20. Trunk, R.; Henn, T.; Dörfler, W.; Nirschl, H.; Krause, M.J. Inertial dilute particulate fluid flow simulations with an Euler–Euler lattice Boltzmann method. *J. Comput. Sci.* **2016**, *17*, 438–445. [CrossRef]
21. Maier, M.L.; Henn, T.; Thäter, G.; Nirschl, H.; Krause, M.J. Multiscale Simulation with a Two-Way Coupled Lattice Boltzmann Method and Discrete Element Method. *Chem. Eng. Technol.* **2017**, *40*, 1591–1598. [CrossRef]
22. Gaedtke, M.; Hoffmann, T.; Reinhardt, V.; Thäter, G.; Nirschl, H.; Krause, M. Flow and heat transfer simulation with a thermal large eddy lattice Boltzmann method in an annular gap with an inner rotating cylinder. *Int. J. Mod. Phys. C* **2019**, *30*, 1950013. [CrossRef]

23. Haussmann, M.; Simonis, S.; Nirschl, H.; Krause, M.J. Direct numerical simulation of decaying homogeneous isotropic turbulence—numerical experiments on stability, consistency and accuracy of distinct lattice Boltzmann methods. *Int. J. Mod. Phys. C* **2019**, *30*, 1–29. [[CrossRef](#)]
24. Simonis, S.; Frank, M.; Krause, M.J. On relaxation systems and their relation to discrete velocity Boltzmann models for scalar advection–diffusion equations. *Philos. Trans. R. Soc. Lond. Ser. A Math. Phys. Eng. Sci.* **2020**, *378*, 20190400. [[CrossRef](#)] [[PubMed](#)]
25. Dapelo, D.; Simonis, S.; Krause, M.J.; Bridgeman, J. Lattice-Boltzmann coupled models for advection–diffusion flow on a wide range of Péclet numbers. *J. Comput. Sci.* **2021**, *51*, 101363. [[CrossRef](#)]
26. Haussmann, M.; Reinshaus, P.; Simonis, S.; Nirschl, H.; Krause, M.J. Fluid–Structure Interaction Simulation of a Coriolis Mass Flowmeter Using a Lattice Boltzmann Method. *Fluids* **2021**, *6*, 167. [[CrossRef](#)]
27. Simonis, S.; Haussmann, M.; Kronberg, L.; Dörfler, W.; Krause, M.J. Linear and brute force stability of orthogonal moment multiple-relaxation-time lattice Boltzmann methods applied to homogeneous isotropic turbulence. *Philos. Trans. R. Soc. Lond. Ser. A Math. Phys. Eng. Sci.* **2021**, *379*, 20200405. [[CrossRef](#)]
28. Siodlaczek, M.; Gaedtke, M.; Simonis, S.; Schweiker, M.; Homma, N.; Krause, M.J. Numerical evaluation of thermal comfort using a large eddy lattice Boltzmann method. *Build. Environ.* **2021**, *192*, 107618. [[CrossRef](#)]
29. Bukreev, F.; Simonis, S.; Kummerländer, A.; Jeßberger, J.; Krause, M.J. Consistent lattice Boltzmann methods for the volume averaged Navier–Stokes equations. *arXiv* **2022**, arXiv:2208.09267.
30. Simonis, S.; Frank, M.; Krause, M.J. Constructing relaxation systems for lattice Boltzmann methods. *arXiv* **2022**, arXiv:2208.14976.
31. Simonis, S.; Krause, M.J. Forschungsnahe Lehre unter Pandemiebedingungen. *Mitteilungen Dtsch. Math.-Ver.* **2022**, *30*, 43–45. [[CrossRef](#)]
32. Simonis, S.; Krause, M.J. Limit Consistency for Lattice Boltzmann Equations. *arXiv* **2022**, arXiv:2208.06867.
33. Simonis, S.; Nguyen, J.; Avis, S.J.; Dörfler, W.; Krause, M.J. Binary mixture flow with free energy lattice Boltzmann methods. *PAMM* **2022**, *22*, e202200025. [[CrossRef](#)]
34. Simonis, S.; Oberle, D.; Gaedtke, M.; Jenny, P.; Krause, M.J. Temporal large eddy simulation with lattice Boltzmann methods. *J. Comput. Phys.* **2022**, *454*, 110991. [[CrossRef](#)]
35. Krause, M.J.; Kummerländer, A.; Avis, S.J.; Kusumaatmaja, H.; Dapelo, D.; Klemens, F.; Gaedtke, M.; Hafen, N.; Mink, A.; Trunk, R.; et al. OpenLB—Open source lattice Boltzmann code. *Comput. Math. Appl.* **2021**, *81*, 258–288. [[CrossRef](#)]
36. Krause, M.; Mink, A.; Trunk, R.; Klemens, F.; Maier, M.L.; Mohrhard, M.; Claro Barreto, A.; Haußmann, M.; Gaedtke, M.; Ross-Jones, J. OpenLB Release 1.2: Open Source Lattice Boltzmann Code, 2018. Available online: <https://www.openlb.net/wp-content/uploads/2018/02/olb-1.2r0.tgz> (accessed on 17 October 2022). [[CrossRef](#)]
37. Cercignani, C. *The Boltzmann Equation and Its Applications*; Applied Mathematical Sciences; Springer: New York, NY, USA, 1987.
38. Babovsky, H. *Die Boltzmann-Gleichung: Modellbildung–Numerik–Anwendungen*; Leitfäden der angewandten Mathematik und Mechanik; Vieweg+Teubner Verlag: Wiesbaden, Germany, 2013.
39. Aidun, C.K.; Clausen, J.R. Lattice-Boltzmann method for complex flows. *Annu. Rev. Fluid Mech.* **2010**, *42*, 439–472. [[CrossRef](#)]
40. Krüger, T.; Kusumaatmaja, H.; Kuzmin, A.; Shardt, O.; Silva, G.; Viggien, E.M. *The Lattice Boltzmann Method*; Springer: Cham, Switzerland, 2017.
41. Modest, M.F. *Radiative Heat Transfer*; Academic Press: Cambridge, MA, USA, 2013.
42. Chandrasekhar, S. *Radiative Transfer*; Clarendon Press: Oxford, UK, 1950; reprinted by Dover Publications, 1960.
43. Huang, Q.; Yao, L.; Liu, T.; Yang, J. Simulation of the light evolution in an annular photobioreactor for the cultivation of Porphyridium cruentum. *Chem. Eng. Sci.* **2012**, *84*, 718–726. [[CrossRef](#)]
44. McHardy, C.; Horneber, T.; Rauh, C. Spectral simulation of light propagation in participating media by using a lattice Boltzmann method for photons. *Appl. Math. Comput.* **2018**, *319*, 59–70. [[CrossRef](#)]
45. Berberoglu, H.; Gomez, P.S.; Pilon, L. Radiation characteristics of *Botryococcus braunii*, *Chlorococcum littorale*, and *Chlorella* sp. used for fixation and biofuel production. *J. Quant. Spectrosc. Radiat. Transf.* **2009**, *110*, 1879–1893. [[CrossRef](#)]
46. Kandilian, R.; Soulies, A.; Pruvost, J.; Rousseau, B.; Legrand, J.; Pilon, L. Simple method for measuring the spectral absorption cross-section of microalgae. *Chem. Eng. Sci.* **2016**, *146*, 357–368. [[CrossRef](#)]
47. McHardy, C.; Luzi, G.; Lindenberger, C.; Agudo, J.R.; Delgado, A.; Rauh, C. Numerical analysis of the effects of air on light distribution in a bubble column photobioreactor. *Algal Res.* **2018**, *31*, 311–325. [[CrossRef](#)]
48. Berberoglu, H.; Yin, J.; Pilon, L. Light transfer in bubble sparged photobioreactors for H₂ production and CO₂ mitigation. *Int. J. Hydrog. Energy* **2007**, *32*, 2273–2285. [[CrossRef](#)]
49. Kandilian, R.; Pruvost, J.; Artu, A.; Lemasson, C.; Legrand, J.; Pilon, L. Comparison of experimentally and theoretically determined radiation characteristics of photosynthetic microorganisms. *J. Quant. Spectrosc. Radiat. Transf.* **2016**, *175*, 30–45. [[CrossRef](#)]
50. Henn, T.; Thäter, G.; Dörfler, W.; Nirschl, H.; Krause, M.J. Parallel dilute particulate flow simulations in the human nasal cavity. *Comput. Fluids* **2016**, *124*, 197–207. [[CrossRef](#)]
51. Béchet, Q.; Shilton, A.; Guieysse, B. Modeling the effects of light and temperature on algae growth: State of the art and critical assessment for productivity prediction during outdoor cultivation. *Biotechnol. Adv.* **2013**, *31*, 1648–1663. [[CrossRef](#)]
52. Lee, E.; Jalalizadeh, M.; Zhang, Q. Growth kinetic models for microalgae cultivation: A review. *Algal Res.* **2015**, *12*, 497–512. [[CrossRef](#)]

53. Darvehei, P.; Bahri, P.A.; Moheimani, N.R. Model development for the growth of microalgae: A review. *Renew. Sustain. Energy Rev.* **2018**, *97*, 233–258. [[CrossRef](#)]
54. Bouzidi, M.; Firdaouss, M.; Lallemand, P. Momentum transfer of a Boltzmann-lattice fluid with boundaries. *Phys. Fluids* **2001**, *13*, 3452–3459. [[CrossRef](#)]
55. Gupta, A. Transport and Hydrodynamic Stresses in Turbulent Flows with Application to Photo-Bioreactors. Ph.D. Thesis, Technische Universiteit Eindhoven, Eindhoven, The Netherlands, 2019.
56. Mink, A. A Comprehensive Computational Model for Coupled Fluid Flow, Mass Transfer and Light Supply in Photobioreactors with Lattice Boltzmann Methods. Ph.D. Thesis, Karlsruher Institut für Technologie (KIT), Karlsruhe, Germany, 2022. [[CrossRef](#)]
57. Kummerländer, A.; Avis, S.; Kusumaatmaja, H.; Bukreev, F.; Dapelo, D.; Großmann, S.; Hafen, N.; Holeksa, C.; Husfeldt, A.; Jeßberger, J.; et al. OpenLB Release 1.5: Open Source Lattice Boltzmann Code, 2022. Available online: <https://www.openlb.net/wp-content/uploads/2022/04/olb-1.5r0.tgz> (accessed on 17 October 2022). [[CrossRef](#)]